JACS Au
AN OPEN ACCESS JOURNAL OF THE AMERICAN CHEMICAL SOCIETY

pubs.acs.org/jacsau

Article

Macrophage-Encapsulated Bioorthogonal Nanozymes for Targeting Cancer Cells

Riddha Das, Joseph Hardie, Bishnu P. Joshi, Xianzhi Zhang, Aarohi Gupta, David C. Luther, Stefano Fedeli, Michelle E. Farkas,* and Vincent M. Rotello*

Cite This: *JACS Au* 2022, 2, 1679−1685

Read Online

ACCESS | Metrics & More | Article Recommendations | Supporting Information

ABSTRACT: Macrophages migrate to tumor sites by following chemoattractant gradients secreted by tumor cells, providing a truly active targeting strategy for cancer therapy. However, macrophage-based delivery faces challenges of cargo loading, control of release, and effects of the payload on the macrophage vehicle. We present a strategy that employs bioorthogonal "nanozymes" featuring transition metal catalysts (TMCs) to provide intracellular "factories" for the conversion of prodyes and prodrugs into imaging agents and chemotherapeutics. These nanozymes solubilize and stabilize the TMCs by embedding them into self-assembled monolayer coating gold nanoparticles. Nanozymes delivered into macrophages were intracellularly localized and retained activity even after prolonged (72 h) incubation. Significantly, nanozyme-loaded macrophages maintained their inherent migratory ability toward tumor cell chemoattractants, efficiently killing cancer cells in cocultures. This work establishes the potential of nanozyme-loaded macrophages for tumor site activation of prodrugs, providing readily tunable dosages and delivery rates while minimizing off-target toxicity of chemotherapeutics.

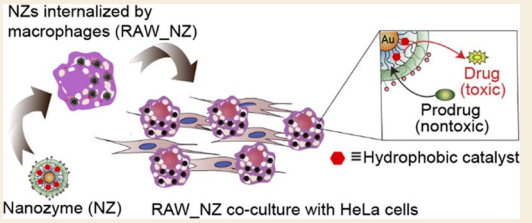

KEYWORDS: *chemotherapy, gold nanoparticles, catalyst, cell-based delivery, bioorthogonal, tumor*

Downloaded via UNIV OF MILAN on September 24, 2024 at 10:23:52 (UTC).
See https://pubs.acs.org/sharingguidelines for options on how to legitimately share published articles.

Drug targeting can reduce off-target toxicity, improving survival time and quality of life for cancer patients.[1−4] Recent metanalyses, however, have shown that the tumor targeting efficiency of most delivery systems is quite low[5−8] and that much of the delivered therapeutic payloads are taken up by tumor-associated macrophages rather than the targeted tumor cells.[9−11] Cell-based therapies provide a potential strategy for the enhanced targeting of tumors.[12−18] However, commonly used cellular vehicles face challenges for tumor targeting.[19,20] Macrophages are inherently attracted to specific tissue environments, including hypoxic, ischemic, and necrotic areas associated with tumors.[21−23] Concurrently, this homing ability is complemented by the secretion of macrophage chemoattractants by many cancer cell types to recruit macrophages to tumors[24,25] that can contribute up to 50% of tumor mass.[26] Taken together, these characteristics make macrophages particularly attractive for use as cell-based delivery vehicles for treating solid tumors that are difficult to reach using conventional targeting strategies.[13,15,27]

Previous therapeutic delivery studies using macrophages as cell-based carriers have loaded them with nanoparticle−drug conjugates or free chemotherapeutics.[14,16,17] These agents provided greater efficacy and reduced off-target toxicity when compared with free drugs.[17,21] The direct loading of therapeutics into macrophages is challenging, however, due to limitations in the amounts of therapeutics that can be loaded into the cells before compromising their viability and/or homing efficiency.[28] To a certain extent, these issues can be addressed by utilizing macrophages bearing stimuli-responsive nanoparticles that control the release of therapeutics.[29,30] In these approaches, external stimuli such as thermal energy, light, or ultrasound can be used to trigger the release of drug molecules from nanoparticles specifically at the tumor site. While this strategy is promising, limited loading and increased complexity of the release process remain as challenges.

Bioorthogonal catalysis[31−37] provides a strategy for creating drug "factories" for on-site activation of pro-imaging agents and prodrugs,[38−40] providing essentially unlimited quantities of active entities at desired cells, tissues, and organs.[41−44] We report here the integration of on-site manufacturing capability with the inherent homing properties of macrophages using cell-internalized bioorthogonal nanozymes (NZs).[45,46] These NZs use gold nanoparticles (AuNPs) to solubilize and stabilize transition metal catalysts (TMCs) through encapsulation in the AuNP monolayer. The TMCs can then generate imaging and therapeutic agents via bioorthogonal uncaging of inactive small molecule precursors in cells.[47−54] NZs were delivered

Received: April 21, 2022
Revised: June 22, 2022
Accepted: June 23, 2022
Published: July 7, 2022

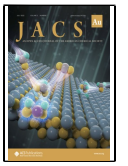

© 2022 The Authors. Published by American Chemical Society

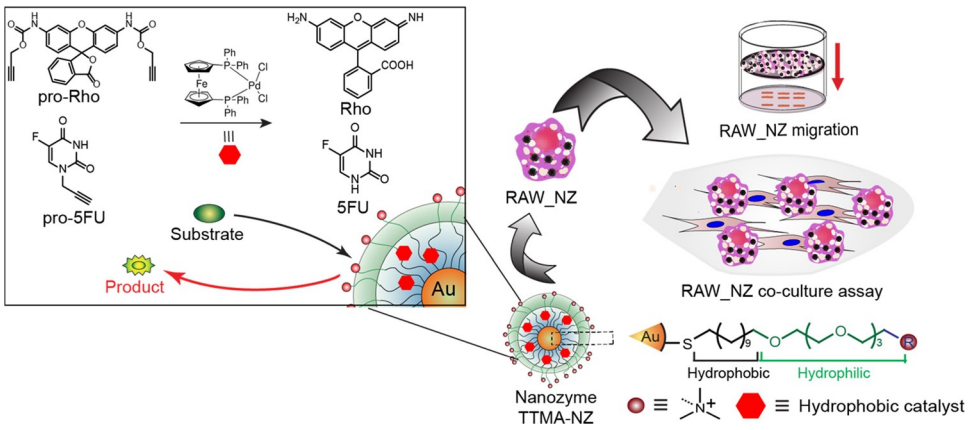

Figure 1. Schematic representation of macrophage-mediated delivery of bioorthogonal nanozymes (**TTMA-NZ**) for prodrug (**pro-5FU**) and pro-fluorophore (**pro-Rho**) activation selectively at tumor cells.

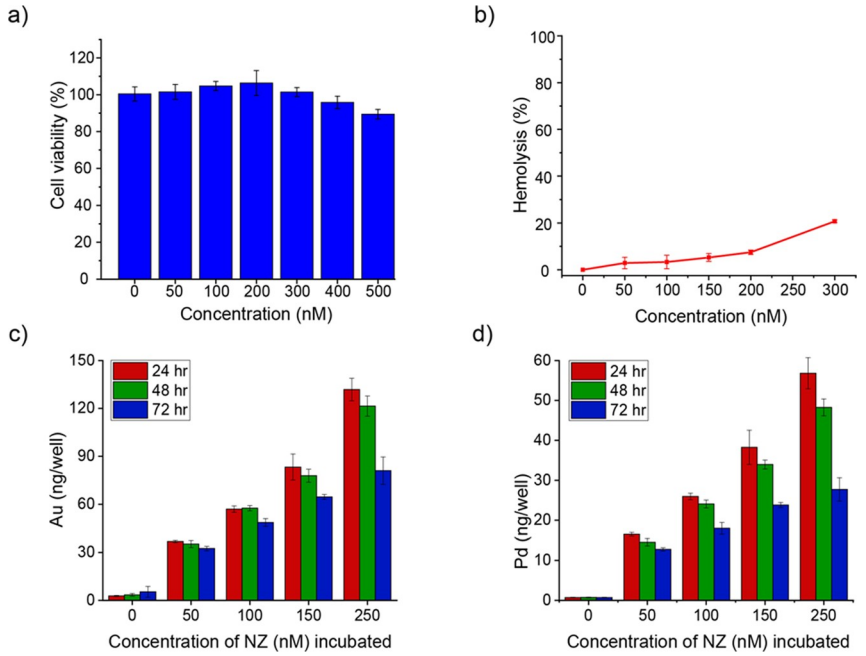

Figure 2. (a) Cytotoxicity of NZs on HeLa cells. (b) Hemolysis of red blood cells by different concentrations of **TTMA-NZ**. (c and d) Retention of NZs in macrophages after prolonged incubation time. Data from ICP-MS evaluation of (c) Au (ng/well) and (d) Pd (ng/well) nanozyme components in RAW 264.7 macrophages (20,000 cells/well) indicate retention after 24, 48, and 72 h incubations. The data shown are averages of experimental triplicates; error bars indicate standard deviations.

into RAW 264.7 macrophages to provide NZ-loaded macrophages (**RAW_NZ**). The efficacy of **RAW_NZ** for pro-fluorophore and prodrug activation was demonstrated in a coculture model with HeLa (human cervical cancer) cells. Macrophages retain their migratory behavior toward colony stimulating factor-1 (CSF-1), a major chemoattractant secreted by cancer cells to recruit macrophages at tumor sites.[55] Significant cancer cell toxicity was achieved in the presence of NZ-bearing macrophages, even at the lowest concentration of the prodrug administered. Taken together, this strategy integrates the targeting ability of cell-based drug delivery with the on-site generation of therapeutics, providing a new approach for targeted drug delivery systems.[56]

RESULTS AND DISCUSSION

Fabrication of Nanozymes

The NZ scaffold was provided by 2 nm cationic AuNPs functionalized with thioalkyl tetra(ethylene glycol) trimethylammonium (**TTMA**), previously shown to have both high cellular uptake and low toxicity.[57−61] The ligand monolayer of **TTMA** contains a crucial hydrophobic alkane interior for catalyst encapsulation and a tetra(ethylene glycol) spacer to provide biocompatibility and improve stability in aqueous intracellular environments (Figure 1). **TTMA** particles were generated from pentanethiol-capped 2 nm core AuNPs using a place exchange reaction (synthesis and characterization of NPs are described in the Supporting Information and Supporting Information Figures S1−S3).[62,63]

Nanozyme **TTMA-NZ** was generated by immobilizing a hydrophobic palladium TMC (1,1′bis(diphenylphosphino)-ferrocene)palladium(II)dichloride[64−66] in the hydrophobic

https://doi.org/10.1021/jacsau.2c00247
JACS Au 2022, 2, 1679−1685

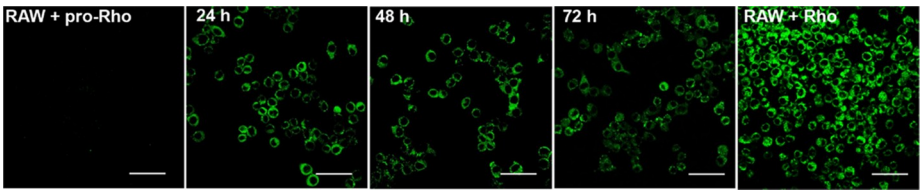

Figure 3. Confocal images of pro-rhodamine 110 fluorophore (**pro-Rho**) activation by **RAW_NZ. RAW_NZ** was generated for 24, 48, and 72 h before the addition of **pro-Rho**. In each case, images were acquired 24 h following exposure of nanozyme to pro-fluorophore. **Pro-Rho** was used as the negative control, and **Rho** was used as the positive control. The scale bars are 15 μm.

portion of AuNP monolayers.[47] In practice, the catalyst was dissolved in acetone and added into an aqueous solution of AuNPs in a 1:1 ratio by volume. Acetone was evaporated slowly, and the excess catalyst was filtered away to provide the desired **TTMA-NZ** (details of NZ preparation and characterization are provided in the Supporting Information). There was no aggregation observed before or after encapsulation of TMCs, as confirmed by dynamic light scattering (Table S1 and Figure S4) and transmission electron microscopy (Figure S5). Quantification of Pd relative to Au by inductively coupled plasma mass spectrometry (ICP-MS) (Table S2) indicated that 37 ± 1 catalysts were present per AuNP.

Loading of Nanozymes into Macrophages

The toxicity of NZs to macrophages (RAW 264.7) was studied, with little effect on cell viability observed over a wide range of concentrations after 24 h incubation, as determined by Alamar blue assay (Figure 2a). We next performed hemolysis assays to further test the safety of NZs. As shown in Figure 2b, **TTMA-NZ** caused minimal hemolysis to human RBCs up to 300 nM. For the cellular uptake study, macrophages were incubated with **TTMA-NZ** for 24 h and then washed with phosphate-buffered saline (PBS) three times to remove noninternalized NZs. The use of additional washes has been shown to remove essentially all externally adsorbed NZs.[67] This process did not affect the effective internalization of **TTMA-NZ**, as determined by ICP-MS analyses of the levels of Au or Pd present in the macrophages (Figure S6). As expected, the resulting **RAW_NZ** macrophages feature Au/Pd ratios consistent with those of the precursor **TTMA-NZ** (Figures 2c,d and S6). The NZ content can be readily tuned through variation in **TTMA-NZ** concentrations during incubation, providing a ~fourfold difference in the NZ level for **RAW_NZ-50 nM** versus **RAW_NZ-250 nM** after incubation. Significantly, retention of Au and Pd was observed over extended (48 and 72 h) periods (Figure 2c,d).

Catalytic Activity of Nanozymes in Living Cells

Effective application of NZ-based cell therapy requires the intracellular activation of substrates. The cell-internalized catalysts of **RAW_NZ** were used to uncage nonfluorescent di(propargyloxycarbonyl)-caged rhodamine 110 (**pro-Rho**)[65] as a pro-fluorophore. **RAW_NZ** was cultured in serum-containing media for 24, 48, or 72 h, followed by addition of pro-Rho and incubation for a further 24 h. Confocal microscopy imaging indicated that **RAW_NZ** successfully activated pro-Rho to rhodamine 110, independent of **RAW_NZ** generation time (Figures 3 and S7). Efficient NZ activity was observed even after 72 h of cell internalization, consistent with the presence of NZ components observed via ICP-MS (Figure 2). Taken together, NZs in **RAW_NZ** both remain inside of macrophages and retain their activity for prolonged periods.

Efficient Chemotactic Migration of RAW_NZ

We next investigated the effects of NZ internalization on macrophage response to chemotactic signals. CSF-1 was used as the chemoattractant, and migration was evaluated by transwell membrane (Boyden Chamber) assay[23] (Figure 4). We compared the abilities of nonmodified macrophages (RAW 264.7) without an NZ versus those loaded with an NZ

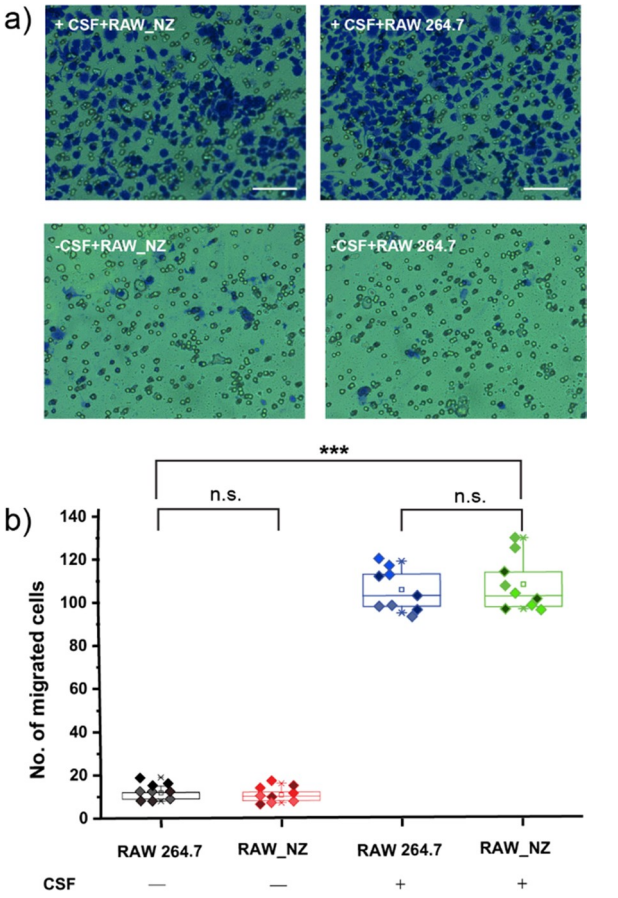

Figure 4. Chemotaxis capabilities are retained by **RAW_NZ** as determined by transwell membrane assay. (a) Confocal imaging of migrated macrophages with NZs (**RAW_NZ**) and without NZs (RAW 264.7) in the presence and absence of chemoattractant CSF-1. All cells were stained with crystal violet to facilitate detection. Scale bar = 100 μm. (b) Quantification of migrated RAW 264.7 cells and **RAW_NZ** in the presence and absence of CSF-1. Nine panels of cells were counted per treatment (n = 9, from three biological replicates). The box constitutes the interquartile range (25th to 75th percentile), the intersecting line designates the median, the small square in the center represents the mean, and the bottom and top whiskers specify the 5th and 95th percentiles, respectively. n.s. = not significant, ***p < 0.0001.

https://doi.org/10.1021/jacsau.2c00247
JACS Au 2022, 2, 1679−1685

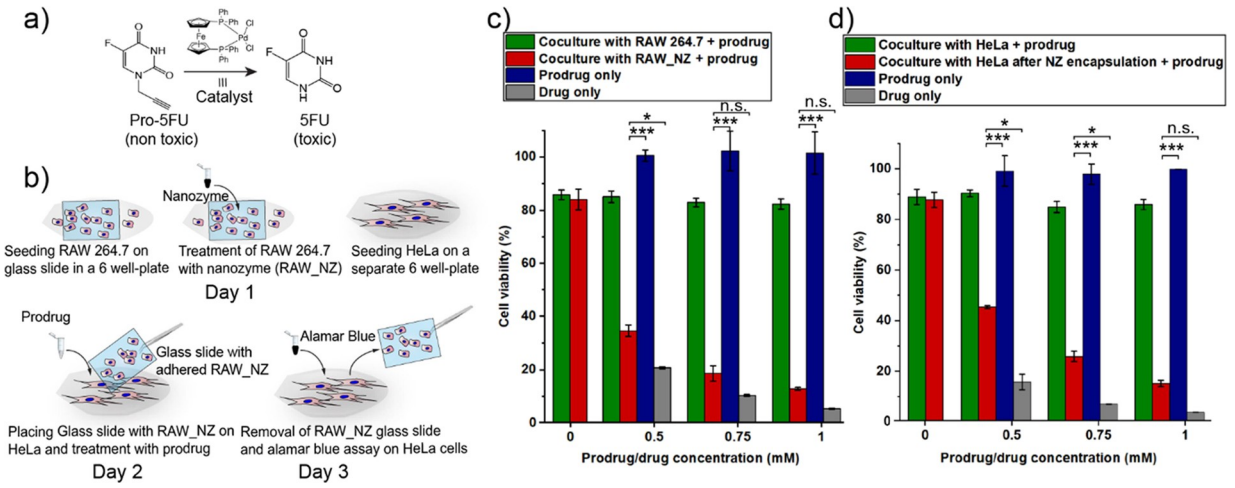

Figure 5. 5FU activation in a coculture system with **RAW_NZ**. (a) Pro-5FU activation by TTMA catalysis. (b) Graphical scheme of the coculture experiment to evaluate therapeutic efficacy of **RAW_NZ** in HeLa cells. Viability of (c) HeLa cells and (d) RAW 264.7 cells following pro-5FU (pro-drug) activation by **RAW_NZ** in the coculture experiment and control conditions. The data are average of triplicates, and the error bars indicate standard deviations. n.s. = not significant, *$p < 0.05$, ***$p < 0.001$.

(**RAW_NZ**) to traffic through a membrane in response to CSF-1 presence. Macrophages were stained with crystal violet at the conclusion of the experiment to visualize and quantify the migrated cells (the detailed procedure is described in the Supporting Information). No significant differences were observed in the behaviors of macrophages (Figure 4b), in the presence or absence of CSF-1, indicating that the NZs do not affect the migratory behavior and chemotaxis capabilities of the macrophages. These *in vitro* Boyden chamber chemotaxis assays demonstrate that the migratory ability of the NZ-loaded macrophage (**RAW_NZ**) is consistent with that of untreated cells (RAW 264.7). As seen in the transwell images and the corresponding plots, the cell migration of the NZ-loaded macrophages and untreated cells toward chemoattractants was found to be essentially identical.

RAW_NZ Kills Cancer Cells in Coculture Models

Having established the stability and retention of inherent chemotactic capabilities of macrophages of **RAW_NZ**s, we next investigated their therapeutic potential in a coculture model with HeLa cells (Figure 5). For this study, propargyl-protected 5-fluorouracil (**pro-5FU**)[66] was chosen as a model prodrug due to the broad application of its active counterpart (**5FU**; Figure 5a).[68,69] The caged propargyl group blocks the active site of **5FU**, reducing cytotoxicity ∼500-fold (Figure S8). The activation of **pro-5FU** was first studied in PBS solution and demonstrated by checking the thin layer chromatography (TLC, Figure S9). The reaction mixture was further analyzed using electrospray ionization mass spectrometry. The presence of the **5FU** peak (m/z 129) indicates the successful activation of **pro-5FU** by NZs (Figure S10). For the coculture experiment, **RAW_NZ** or RAW 264.7 cells were seeded on glass slides that were then immersed into wells seeded with HeLa cells (Figure 5b). Macrophage-free slides and HeLa-free wells were used for additional control conditions. **Pro-5FU** (0 to 1 mM) was added to the coculture and control wells and incubated for 24 h. Slides with **RAW_NZ** and controls were removed before performing Alamar blue assays separately on HeLa cells and macrophages to differentiate viabilities by the cell type (details provided in the Supporting Information). In the presence of **RAW_NZ**, the viabilities of both HeLa (Figure 5c) and RAW 264.7 carrier (Figure 5d) cells were substantially reduced with increasing concentrations of the prodrug. This dose-dependent cytotoxicity indicates the successful conversion of pro-5FU into the active therapeutic by NZs. The activity against the HeLa cells demonstrates that the uncaged drug was able to diffuse from the macrophages to the target cells. HeLa (and macrophage) cells that received increasing concentrations of prodrug but were not cultured with **RAW_NZ** (or **TTMA-NZ**) did not show any reduction in cell viability, indicating successful caging of 5FU (Figure 5c,d). **RAW_NZ** was also cocultured with green fluorescent protein (GFP) expressing HeLa cells (GFP-HeLa) and separately, U2OS cells (GFP-U2OS). In these experiments, the toxicity of the activated prodrug toward target cancer cells was assessed via monitoring of fluorescent signals. The green fluorescence of both GFP-HeLa cells and GFP-U2OS cells was greatly reduced with the increasing concentration of prodrug (Figure S11), indicating cell death and effective therapeutic activity against both cell lines.

Carrier cell death is not an issue in the therapeutic setting, so long as it occurs after the target tissue has been reached. Diminished viability of RAW 264.7 cells was observed only in treatments where the NZ and prodrug were both present. Likewise, free NZs and AuNPs were nontoxic to cancer cells in the absence of the prodrug. NZs showed toxicity only in the presence of the prodrug, whereas AuNPs remained nontoxic at all prodrug concentrations (Figure S11). In related experiments, **RAW_NZ** was compared to free **TTMA-NZ** to evaluate whether cellular loading affects the catalytic activity of the agents with similar activity observed for the NZ and **RAW_NZ** (Figure S12). Based on our previous research,[23] we are optimistic about the targeting efficiency of macrophages toward the tumor; however, liver accumulation should be considered as a potential challenge. Dosing of the prodrug is expected to not be an issue since this **5FU** prodrug has been used at the levels used for our studies recently *in vivo*, showing no toxicity to mice.[70]

CONCLUSIONS

In summary, we have demonstrated a macrophage-based bioorthogonal strategy for tumor imaging and therapy. Macrophages bearing internalized bioorthogonal NZs featured

https://doi.org/10.1021/jacsau.2c00247
JACS Au 2022, 2, 1679−1685

catalytic activity extending over days. The carrier macrophages retained chemotactic behavior and exhibited efficient generation of therapeutics in a coculture model, illustrating the potential of this macrophage-based therapy for therapeutic uses. Coupling the chemotactic ability of macrophages and the ability to generate therapeutic and imaging agents at tumor sites presents a new strategy for reducing off-target effects and extending on-demand delivery, providing the potential to bring drug-activating factories into tumors. Future studies are underway exploring the use of this platform for specific drug activation in *in vivo* tumor models.

METHODS

Fabrication of Nanozymes

The catalyst was dissolved in acetone (2 mg/mL) and mixed with **AuNPs** in a 1:1 ratio by volume. The organic layer was slowly evaporated. The resulting mixture was filtered using a syringe-driven filter unit (pore size = 0.2 μm). The excess catalyst was removed via multiple filtrations through a molecular weight cut-off filter (10 K), followed by dialysis.[49]

Preparation of Engineered Macrophages (RAW_NZ)

Macrophages (RAW 264.7) were seeded at a concentration of 20,000 cells/well in a 24 well plate and allowed to attach overnight (at 37 °C in a humidified atmosphere of 5% CO_2). After 24 h, cells were washed three times with PBS to remove any dead cells. **NZ** solution (100 nM) in macrophage growth media (described above) was added to the cells and incubated together for 24 h (at 37 °C in a humidified atmosphere of 5% CO_2), except where otherwise noted for specific experiments. After this, the cells were washed with PBS three times to remove any excess **NZ**, to provide **RAW_NZ**. **RAW_NZ** was detached via treatment with trypsin, depending on the nature of the experiment to follow.

Chemotaxis/Boyden Chamber Assay

Cell migration toward CSF-1 was investigated by a Boyden chamber assay following previously described protocols.[23,71] Briefly, a transwell membrane with 8 mm pore size was coated with 10 mg/mL fibronectin. After 4 h, the excess fibronectin was rinsed with PBS and left to dry overnight. The next day, designated wells of a 24-well plate received 650 mL of serum-free growth media supplemented with 40 ng/mL rCSF-1; control wells received serum-free growth media only. The fibronectin-coated inserts were then placed onto the wells. Next, 100 mL of **RAW_NZ** (100,000 cells/well) solution was added into each insert and incubated for 12 h at 37 °C and 5% CO_2. Nonmigratory cells were removed with a Q-tip, and migratory cells at the bottom of the inserts were fixed in 4% formaldehyde and stained with a 0.1% crystal violet solution in 25% methanol. Membranes were removed precisely, mounted onto cover-glass, and visualized under a Zeiss Axio Observer Z1 with an Axio Cam 506 Color attachment under a 20× objective lens. The cells were counted from three random, nonoverlapping fields of view per membrane, with three membranes per condition ($n = 3 \times 3 = 9$). Box and whisker plots were generated using OriginPro 2017.

Coculture of RAW_NZ with HeLa Cells and Viability Evaluation

Glass slides were coated with poly-lysine solution, washed with PBS, and dried overnight. Each of the dry glass slides was placed onto each well of a 6-well plate. Macrophages (RAW 264.7) (100,000/well) in standard growth media were seeded in designated wells with glass slides; 3 mL of media was used in each well to ensure that the glass slides remained fully immersed in solution. The cells were treated with 100 nM NZs for wells designated as **RAW_NZ**. In parallel, HeLa cells (100,000/well) were seeded in separate 6-well plates. All plates were stored under 5% CO_2 at 37 °C for 24 h. HeLa cells were washed three times with PBS followed by adding fresh, standard growth media. The glass slides coated with RAW 264.7/**RAW_NZ** were thoroughly washed with PBS to remove any nonadhered cells and/or excess NZ. The slides were then removed carefully with a tweezer from their designated wells and placed within wells containing HeLa cells (atop the cells) for coculture. As a result, both HeLa cells and RAW 264.7/**RAW_NZ** were in the same wells and solution. For control experiments with only HeLa cells, blank glass slides were placed on top of the cells. For control experiments with only RAW 264.7 cells, the slides coated with RAW 264.7 cells were placed in wells containing only media. The cells were incubated with the prodrug/drug for 24 h, followed by washing three times with PBS. The glass slides were removed and placed in separate 6-well plates. All wells (with cells now separated) were thoroughly washed with PBS three times. Finally, 10% Alamar blue assay in serum-containing media was performed separately for HeLa and RAW 264.7 cells.

ASSOCIATED CONTENT

Supporting Information

The Supporting Information is available free of charge at https://pubs.acs.org/doi/10.1021/jacsau.2c00247.

Preparation and characterization of nanozymes, quantification of catalytic activity, and cell studies (PDF)

AUTHOR INFORMATION

Corresponding Authors

Michelle E. Farkas − *Department of Chemistry, University of Massachusetts Amherst, Amherst, Massachusetts 01003, United States;* orcid.org/0000-0001-5824-1243; Phone: (+1) 413−545-2058; Email: farkas@chem.umass.edu; Fax: (+1) 413−545-2058

Vincent M. Rotello − *Department of Chemistry, University of Massachusetts Amherst, Amherst, Massachusetts 01003, United States;* orcid.org/0000-0002-5184-5439; Phone: (+1) 413−545-2058; Email: rotello@chem.umass.edu; Fax: (+1) 413−545-2058

Authors

Riddha Das − *Department of Chemistry, University of Massachusetts Amherst, Amherst, Massachusetts 01003, United States*

Joseph Hardie − *Department of Chemistry, University of Massachusetts Amherst, Amherst, Massachusetts 01003, United States*

Bishnu P. Joshi − *Department of Chemistry, University of Massachusetts Amherst, Amherst, Massachusetts 01003, United States*

Xianzhi Zhang − *Department of Chemistry, University of Massachusetts Amherst, Amherst, Massachusetts 01003, United States;* orcid.org/0000-0002-9585-7458

Aarohi Gupta − *Department of Chemistry, University of Massachusetts Amherst, Amherst, Massachusetts 01003, United States;* orcid.org/0000-0003-1303-1159

David C. Luther − *Department of Chemistry, University of Massachusetts Amherst, Amherst, Massachusetts 01003, United States;* orcid.org/0000-0002-4697-8683

Stefano Fedeli − *Department of Chemistry, University of Massachusetts Amherst, Amherst, Massachusetts 01003, United States*

Complete contact information is available at: https://pubs.acs.org/10.1021/jacsau.2c00247

Notes

The authors declare no competing financial interest.

https://doi.org/10.1021/jacsau.2c00247
JACS Au 2022, 2, 1679−1685

■ ACKNOWLEDGMENTS

This work was supported by grants from the NIH (EB022641) and NSF (CHE-2108044) to V.M.R. and NIH National Service Award GM008515 to D.C.L. Wide-field fluorescence imaging for chemotaxis studies was performed in the laboratory of Shelly Peyton (UMass Amherst). Confocal imaging was performed in Light Microscopy at the Institute for Applied Life Science (UMass Amherst), with the support from the Massachusetts Life Sciences Center. We would like to thank Ruthanne Paradise and Bill Schmitt for assistance in gathering FTIR results (UMass Amherst). U2OS-GFP expressing cells were provided by Patricia Wadsworth (UMass Amherst).

■ REFERENCES

(1) Danhier, F.; Feron, O.; Préat, V. To Exploit the Tumor Microenvironment: Passive and Active Tumor Targeting of Nanocarriers for Anti-Cancer Drug Delivery. *J. Controlled Release* **2010**, *148*, 135−146.
(2) Byrne, J. D.; Betancourt, T.; Brannon-Peppas, L. Active Targeting Schemes for Nanoparticle Systems in Cancer Therapeutics. *Adv. Drug Delivery Rev.* **2008**, *60*, 1615−1626.
(3) Garzon, R.; Marcucci, G.; Croce, C. M. Targeting MicroRNAs in Cancer: Rationale, Strategies and Challenges. *Nat. Rev. Drug Discovery* **2010**, *9*, 775−789.
(4) Ma, C.; Xia, F.; Kelley, S. O. Mitochondrial Targeting of Probes and Therapeutics to the Powerhouse of the Cell. *Bioconjugate Chem.* **2020**, *31*, 2650−2667.
(5) Rosenblum, D.; Joshi, N.; Tao, W.; Karp, J. M.; Peer, D. Progress and Chanllenges towards Targeted Delivery of Cancer Therapeutics. *Nat. Commun.* **2018**, *9*, 1410.
(6) Wilhelm, S.; Tavares, A. J.; Dai, Q.; Ohta, S.; Audet, J.; Dvorak, H. F.; Chan, W. C. W. Analysis of Nanoparticle Delivery to Tumours. *Nat. Rev. Mater.* **2016**, *1*, 16014.
(7) Lammers, T.; Kiessling, F.; Hennink, W. E.; Storm, G. Drug Targeting to Tumors: Principles, Pitfalls and (Pre-) Clinical Progress. *J. Controlled Release* **2012**, *161*, 175−187.
(8) Sykes, E. A.; Chen, J.; Zheng, G.; Chan, W. C. W. Investigating the Impact of Nanoparticle Size on Active and Passive Tumor Targeting Efficiency. *ACS Nano* **2014**, *8*, 5696−5706.
(9) Miller, M. A.; Zheng, Y.; Gadde, S.; Pfirschke, C.; Zope, H.; Engblom, C.; Kohler, R. H.; Iwamoto, Y.; Yang, K. S.; Askevold, B.; et al. Tumour-Associated Macrophages Act as a Slow-Release Reservoir of Nano-Therapeutic Pt(IV) pro-Drug. *Nat. Commun.* **2015**, *6*, 8692.
(10) Dai, Q.; Wilhelm, S.; Ding, D.; Syed, A. M.; Sindhwani, S.; Zhang, Y.; Chen, Y. Y.; Macmillan, P.; Chan, W. C. W. Quantifying the Ligand-Coated Nanoparticle Delivery to Cancer Cells in Solid Tumors. *ACS Nano* **2018**, *12*, 8423−8435.
(11) Huai, Y.; Hossen, M. N.; Wilhelm, S.; Bhattacharya, R.; Mukherjee, P. Nanoparticle Interactions with the Tumor Microenvironment. *Bioconjugate Chem.* **2019**, *30*, 2247−2263.
(12) Joshi, B. P.; Hardie, J.; Farkas, M. E. Harnessing Biology to Deliver Therapeutic and Imaging Entities via Cell-Based Methods. *Chem. − Eur. J.* **2018**, *24*, 8717−8726.
(13) Pierigè, F.; Serafini, S.; Rossi, L.; Magnani, M. Cell-Based Drug Delivery. *Adv. Drug Delivery Rev.* **2008**, *60*, 286−295.
(14) Choi, M.-R.; Stanton-Maxey, K. J.; Stanley, J. K.; Levin, C. S.; Bardhan, R.; Akin, D.; Badve, S.; Sturgis, J.; Robinson, J. P.; Bashir, R. A Cellular Trojan Horse for Delivery of Therapeutic Nanoparticles into Tumors. *Nano Lett.* **2007**, *7*, 3759−3765.
(15) Doshi, N.; Swiston, A. J.; Gilbert, J. B.; Alcaraz, M. L.; Cohen, R. E.; Rubner, M. F.; Mitragotri, S. Cell-Based Drug Delivery Devices Using Phagocytosis-Resistant Backpacks. *Adv. Healthcare Mater.* **2011**, *23*, H105−H109.
(16) Anselmo, A. C.; Mitragotri, S. Cell-Mediated Delivery of Nanoparticles: Taking Advantage of Circulatory Cells to Target Nanoparticles. *J. Controlled Release* **2014**, *190*, 531−541.
(17) Batrakova, E. V.; Gendelman, H. E.; Kabanov, A. V. Cell-Mediated Drug Delivery. *Expert Opin. Drug Delivery* **2011**, *8*, 415−433.
(18) Wang, Q.; Cheng, H.; Peng, H.; Zhou, H.; Li, P. Y.; Langer, R. Non-genetic engineering of cells for drug delivery and cell-based therapy. *Adv. Drug Delivery Rev.* **2015**, *91*, 125−140.
(19) Sun, X.; Wang, C.; Gao, M.; Hu, A.; Liu, Z. Remotely Controlled Red Blood Cell Carriers for Cancer Targeting and Near-Infrared Light-Triggered Drug Release in Combined Photothermal-Chemotherapy. *Adv. Funct. Mater.* **2015**, *25*, 2386−2394.
(20) Studeny, M.; Marini, F. C.; Champlin, R. E.; Zompetta, C.; Fidler, I. J.; Andreeff, M. Bone Marrow-Derived Mesenchymal Stem Cells as Vehicles for Interferon-β Delivery into Tumors. *Cancer Res.* **2002**, *62*, 3603−3608.
(21) Murdoch, C.; Giannoudis, A.; Lewis, C. E. Mechanisms Regulating the Recruitment of Macrophages into Hypoxic Areas of Tumors and Other Ischemic Tissues. *Blood* **2004**, *104*, 2224−2234.
(22) Brown, J. M.; Giaccia, A. J. The Unique Physiology of Solid Tumors: Opportunities (and Problems) for Cancer Therapy. *Cancer Res.* **1998**, *58*, 1408−1416.
(23) Joshi, B. P.; Hardie, J.; Mingroni, M. A.; Farkas, M. E. Surface-Modified Macrophages Facilitate Tracking of Breast Cancer- Immune Interactions. *ACS Chem. Biol.* **2018**, *13*, 2339−2346.
(24) Pollard, J. W. Tumour-Educated Macrophages Promote Tumour Progression and Metastasis. *Nat. Rev. Cancer* **2004**, *4*, 71−78.
(25) Lewis, C. E.; Pollard, J. W. Distinct Role of Macrophages in Different Tumor Microenvironments. *Cancer Res.* **2006**, *66*, 605−612.
(26) Zhang, Y.; Cheng, S.; Zhang, M.; Zhen, L.; Pang, D.; Zhang, Q.; Li, Z. High-Infiltration of Tumor-Associated Macrophages Predicts Unfavorable Clinical Outcome for Node-Negative Breast Cancer. *PLoS One* **2013**, *8*, No. e76147.
(27) Wan, D. H.; Ma, X. Y.; Lin, C.; Zhu, D. H.; Li, X.; Zheng, B. Y.; Li, J.; Ke, M. R.; Huang, J. D. Noncovalent Indocyanine Green Conjugate of C-Phycocyanin: Preparation and Tumor-Associated Macrophages-Targeted Photothermal Therapeutics. *Bioconjugate Chem.* **2020**, *31*, 1438−1448.
(28) Fu, J.; Wang, D.; Mei, D.; Zhang, H.; Wang, Z.; He, B.; Dai, W.; Zhang, H.; Wang, X.; Zhang, Q. Macrophage Mediated Biomimetic Delivery System for the Treatment of Lung Metastasis of Breast Cancer. *J. Controlled Release* **2015**, *204*, 11−19.
(29) Mura, S.; Nicolas, J.; Couvreur, P. Stimuli-Responsive Nanocarriers for Drug Delivery. *Nat. Mater.* **2013**, *12*, 991−1003.
(30) Ganta, S.; Devalapally, H.; Shahiwala, A.; Amiji, M. A Review of Stimuli-Responsive Nanocarriers for Drug and Gene Delivery. *J. Controlled Release* **2008**, *126*, 187−204.
(31) Sletten, E. M.; Bertozzi, C. R. Bioorthogonal Chemistry: Fishing for Selectivity in a Sea of Functionality. *Angew. Chem., Int. Ed.* **2009**, *48*, 6974−6998.
(32) Völker, T.; Meggers, E. Transition-Metal-Mediated Uncaging in Living Human Cells—an Emerging Alternative to Photolabile Protecting Groups. *Curr. Opin. Chem. Biol.* **2015**, *25*, 48−54.
(33) Völker, T.; Dempwolff, F.; Graumann, P. L.; Meggers, E. Progress towards Bioorthogonal Catalysis with Organometallic Compounds. *Angew. Chem., Int. Ed.* **2014**, *53*, 10536−10540.
(34) Zhang, X.; Huang, R.; Gopalakrishnan, S.; Cao-milán, R.; Rotello, V. M. Bioorthogonal Nanozymes: Progress towards Therapeutic Applications. *Trends Chem.* **2019**, *1*, 90−98.
(35) Bai, Y.; Chen, J.; Zimmerman, S. C. Designed Transition Metal Catalysts for Intracellular Organic Synthesis. *Chem. Soc. Rev.* **2018**, *47*, 1811−1821.
(36) van de L'Isle, M. O. N.; Ortega-Liebana, M. C.; Unciti-Broceta, A. Transition Metal Catalysts for the Bioorthogonal Synthesis of Bioactive Agents. *Curr. Opin. Chem. Biol.* **2021**, *61*, 32−42.
(37) Wang, W.; Zhang, X.; Huang, R.; Hirschbiegel, C. M.; Wang, H.; Ding, Y.; Rotello, V. M. In Situ Activation of Therapeutics

https://doi.org/10.1021/jacsau.2c00247
JACS Au 2022, 2, 1679−1685

through Bioorthogonal Catalysis. *Adv. Drug Delivery Rev.* **2021**, *176*, No. 113893.
(38) Springer, C. J.; Niculescu-Duvaz, I. Prodrug-Activating Systems in Suicide Gene Therapy. *J. Clin. Invest.* **2000**, *105*, 1161−1167.
(39) Denmeade, S. R.; Mhaka, A. M.; Rosen, D. M.; Brennen, W. N.; Dalrymple, S.; Dach, I.; Olesen, C.; Gurel, B.; Demarzo, A. M.; Wilding, G.; et al. Engineering a Prostate-Specific Membrane Antigen − Activated Tumor Endothelial Cell Prodrug for Cancer Therapy. *Sci. Transl. Med.* **2012**, *4*, 140ra86.
(40) Heine, D.; Müller, R.; Brüsselbach, S. Cell Surface Display of a Lysosomal Enzyme for Extracellular Gene-Directed Enzyme Prodrug Therapy. *Gene Ther.* **2001**, *8*, 1005−1010.
(41) Sancho-albero, M.; Rubio-ruiz, B.; Pérez-lópez, A. M.; Sebastián, V.; Martín-duque, P.; Arruebo, M.; Santamaría, J.; Unciti-broceta, A. Cancer-Derived Exosomes Loaded with Ultrathin Palladium Nanosheets for Targeted Bioorthogonal Catalysis. *Nat. Catal.* **2019**, *2*, 864−872.
(42) Du, Z.; Liu, C.; Song, H.; Scott, P.; Liu, Z.; Ren, J.; Qu, X. Neutrophil-Membrane-Directed Bioorthogonal Synthesis of Inflammation-Targeting Chiral Drugs. *Chem* **2020**, *6*, 2060−2072.
(43) Das, R.; Landis, R. F.; Tonga, G. Y.; Cao-Milán, R.; Luther, D. C.; Rotello, V. M. Control of Intra-versus Extracellular Bioorthogonal Catalysis Using Surface-Engineered Nanozymes. *ACS Nano* **2018**, *13*, 229−235.
(44) Gupta, A.; Das, R.; Yesilbag Tonga, G.; Mizuhara, T.; Rotello, V. M. Charge-Switchable Nanozymes for Bioorthogonal Imaging of Biofilm-Associated Infections. *ACS Nano* **2018**, *12*, 89−94.
(45) Huang, Y.; Ren, J.; Qu, X. Nanozymes: Classification , Catalytic Mechanisms, Activity Regulation, and Applications. *Chem. Rev.* **2019**, *119*, 4357−4412.
(46) Wu, J.; Wang, X.; Wang, Q.; Lou, Z.; Li, S.; Zhu, Y.; Qin, L.; Wei, H. Nanomaterials with Enzyme-like Characteristics (Nanozymes): Next-Generation Artificial Enzymes (II). *Chem. Soc. Rev.* **2019**, *48*, 1004−1076.
(47) Tonga, G. Y.; Jeong, Y.; Duncan, B.; Mizuhara, T.; Mout, R.; Das, R.; Kim, S. T.; Yeh, Y.-C.; Yan, B.; Hou, S. Supramolecular Regulation of Bioorthogonal Catalysis in Cells Using Nanoparticle-Embedded Transition Metal Catalysts. *Nat. Chem.* **2015**, *7*, 597.
(48) Cao-Milán, R.; He, L. D.; Shorkey, S.; Tonga, G. Y.; Wang, L.-S.; Zhang, X.; Uddin, I.; Das, R.; Sulak, M.; Rotello, V. M. Modulating the Catalytic Activity of Enzyme-like Nanoparticles through Their Surface Functionalization. *Mol. Syst. Des. Eng.* **2017**, *2*, 624−628.
(49) Jeong, Y.; Tonga, G. Y.; Duncan, B.; Yan, B.; Das, R.; Sahub, C.; Rotello, V. M. Solubilization of Hydrophobic Catalysts Using Nanoparticle Hosts. *Small* **2018**, *14*, No. 1702198.
(50) Zhang, X.; Liu, Y.; Gopalakrishnan, S.; Castellanos-Garcia, L.; Li, G.; Malassine, M.; Uddin, I.; Huang, R.; Luther, D. C.; Vachet, R. W.; et al. Intracellular Activation of Bioorthogonal Nanozymes through Endosomal Proteolysis of the Protein Corona. *ACS Nano* **2020**, *14*, 4767−4773.
(51) Cao-milan, R.; Gopalakrishnan, S.; He, L. D.; Huang, R.; Wang, L.; Castellanos, L.; Luther, D. C.; Landis, R. F.; Makabenta, J. M. V.; Li, C.; et al. Thermally Gated Bio-Orthogonal Nanozymes with Supramolecularly Confined Porphyrin Catalysts for Antimicrobial Uses. *Chem* **2020**, *6*, 1113−1124.
(52) Zhang, X.; Fedeli, S.; Gopalakrishnan, S.; Huang, R.; Gupta, A.; Luther, D. C.; Rotello, V. M. Protection and Isolation of Bioorthogonal Metal Catalysts by Using Monolayer-Coated Nanozymes. *ChemBioChem* **2020**, *21*, 2759−2763.
(53) Zhang, X.; Landis, R. F.; Keshri, P.; Cao-Milán, R.; Luther, D. C.; Gopalakrishnan, S.; Liu, Y.; Huang, R.; Li, G.; Malassiné, M.; et al. Intracellular Activation of Anticancer Therapeutics Using Polymeric Bioorthogonal Nanocatalysts. *Adv. Healthcare Mater.* **2020**, *10*, No. 2001627.
(54) Huang, R.; Li, C.; Cao-milan, R.; He, L. D.; Makabenta, J. M.; Zhang, X.; Yu, E.; Rotello, V. M. Polymer-Based Bioorthogonal Nanocatalysts for the Treatment of Bacterial Biofilms. *J. Am. Chem. Soc.* **2020**, *142*, 10723−10729.
(55) Pixley, F. J.; Stanley, E. R. CSF-1 Regulation of the Wandering Macrophage: Complexity in Action. *Trends Cell Biol.* **2004**, *14*, 628−638.
(56) Hardie, J. M. *Chemical manipulation of macrophages: nanomaterial and molecular approaches*. Ph.D. Dissertation. University of Massachusetts Amherst, Amherst, MA, 2020.
(57) Jiang, Y.; Huo, S.; Mizuhara, T.; Das, R.; Lee, Y.; Hou, S.; Moyano, D. F.; Duncan, B.; Liang, X.; Rotello, V. M. The Interplay of Size and Surface Functionality on the Cellular Uptake of Sub-10 Nm Gold Nanoparticles. *ACS Nano* **2015**, *9*, 9986−9993.
(58) Rana, S.; Bajaj, A.; Mout, R.; Rotello, V. M. Monolayer Coated Gold Nanoparticles for Delivery Applications. *Adv. Drug Delivery Rev.* **2012**, *64*, 200−216.
(59) Saha, K.; Agasti, S. S.; Kim, C.; Li, X.; Rotello, V. M. Gold Nanoparticles in Chemical and Biological Sensing. *Chem. Rev.* **2012**, *112*, 2739−2779.
(60) Ghosh, P.; Han, G.; De, M.; Kim, C. K.; Rotello, V. M. Gold Nanoparticles in Delivery Applications. *Adv. Drug Delivery Rev.* **2008**, *60*, 1307−1315.
(61) Albanese, A.; Tang, P. S.; Chan, W. C. W. The Effect of Nanoparticle Size, Shape, and Surface Chemistry on Biological Systems. *Annu. Rev. Biomed. Eng.* **2012**, *14*, 1−16.
(62) Moyano, D. F.; Duncan, B.; Rotello, V. M. Preparation of 2 nm Gold Nanoparticles for In Vitro and In Vivo Applications. *Methods Mol. Biol.* **2013**, *1025*, 3−8.
(63) Tonga, G. Y.; Mizuhara, T.; Saha, K.; Jiang, Z.; Hou, S.; Das, R.; Rotello, V. M. Binding Studies of Cucurbit[7]uril with Gold Nanoparticles Bearing Different Surface Functionalities. *Tetrahedron Lett.* **2015**, *56*, 3653−3657.
(64) Yusop, R. M.; Unciti-Broceta, A.; Johansson, E. M. V.; Sánchez-Martín, R. M.; Bradley, M. Palladium-Mediated Intracellular Chemistry. *Nat. Chem.* **2011**, *3*, 239−243.
(65) Li, J.; Yu, J.; Zhao, J.; Wang, J.; Zheng, S.; Lin, S.; Chen, L.; Yang, M.; Jia, S.; Zhang, X.; et al. Palladium-Triggered Deprotection Chemistry for Protein Activation in Living Cells. *Nat. Chem.* **2014**, *6*, 352−361.
(66) Weiss, J. T.; Dawson, J. C.; Macleod, K. G.; Rybski, W.; Fraser, C.; Torres-Sánchez, C.; Patton, E. E.; Bradley, M.; Carragher, N. O.; Unciti-Broceta, A. Extracellular Palladium-Catalysed Dealkylation of 5-Fluoro-1-Propargyl-Uracil as a Bioorthogonally Activated Prodrug Approach. *Nat. Commun.* **2014**, *5*, 3277.
(67) Hou, S.; Sikora, K. N.; Tang, R.; Liu, Y.; Lee, Y.-W.; Kim, S. T.; Jiang, Z.; Vachet, R. W.; Rotello, V. M. Quantitative Differentiation of Cell Surface-Bound and Internalized Cationic Gold Nanoparticles Using Mass Spectrometry. *ACS Nano* **2016**, *10*, 6731−6736.
(68) Longley, D. B.; Harkin, D. P.; Johnston, P. G. 5-Fluorouracil: mechanisms of action and clinical strategies. *Nat. Rev. Cancer* **2003**, *3*, 330−338.
(69) Cohen, S. S.; Flaks, J. G.; Barner, H. D.; Loeb, M. R.; Lichtenstein, J. The mode of action of 5-fluorouracil and its derivatives. *Proc. Natl. Acad. Sci. U. S. A.* **1958**, *44*, 1004−1012.
(70) Adam, C.; Bray, T. L.; Pérez-López, A. M.; Tan, E. H.; Rubio-Ruiz, B.; Baillache, D. J.; Houston, D. R.; Salji, M. J.; Leung, H. Y.; Unciti-Broceta, A. A 5-FU Precursor Designed to Evade Anabolic and Catabolic Drug Pathways and Activated by Pd Chemistry in Vitro and in Vivo. *J. Med. Chem.* **2022**, *65*, 552−561.
(71) Suetsugu, A.; Katz, M.; Fleming, J.; Truty, M.; Thomas, R.; Saji, S.; Moriwaki, H.; Bouvet, M.; Hoffman, R. M. Non-invasive Fluorescent-protein Imaging of Orthotopic Pancreatic-cancer-patient Tumorgraft Progression in Nude Mice. *Anticancer Res.* **2012**, *32*, 3063−3067.

https://doi.org/10.1021/jacsau.2c00247
JACS Au 2022, 2, 1679−1685